RJC

RASĀYAN *J. Chem.*
Vol. 18 | No. 4 |2048-2054| October-December | 2025
ISSN: 0974-1496 | e-ISSN: 0976-0083 | CODEN: RJCABP
http://www.rasayanjournal.com
http://www.rasayanjournal.co.in

ECO-FRIENDLY SYNTHESIS OF SNO_2 NANOPARTICLES FROM *Murraya koenigii*: A COMPARATIVE STUDY OF LEAF, STEM, AND ROOT EXTRACTS

Priya Gupta, Hira Ilyas, D. S. Raghav and Sudha Tomar✉
Department of Applied Science and Humanities, Invertis University, Bareilly-243123, (Uttar Pradesh) India
✉Corresponding author: sudhatomar008@gmail.com

ABSTRACT

The present study reports the green synthesis of tin oxide (SnO_2) nanoparticles using different parts-leaf, stem, and root-of *Murraya koenigii* (curry plant) as bioreducing and stabilizing agents. The eco-friendly synthesis was achieved without the use of toxic chemicals, aligning with the principles of green chemistry. Characterization of the synthesized nanoparticles was performed using UV–Visible spectroscopy, X-ray diffraction (XRD), Fourier-transform infrared spectroscopy (FTIR), scanning electron microscopy (SEM), energy-dispersive X-ray spectroscopy (EDS), and thermogravimetric analysis (TGA/DTG). UV–Vis analysis confirmed the nanoscale optical absorption below 400 nm, while XRD revealed the formation of highly crystalline tetragonal rutile SnO_2 with particle sizes ranging from 12–16 nm. FTIR spectra indicated the presence of functional groups associated with phytochemicals involved in the reduction and stabilization process. SEM images displayed distinct surface morphologies influenced by the plant part used, and EDS confirmed the elemental composition with high purity. Thermal analysis showed multi-step degradation behavior, with stem-extract-based SnO_2 (SnO_2-MK#S) exhibiting the highest thermal stability (77.09% residue). Catalytic efficiency was evaluated through the degradation of malachite green dye, where SnO_2-MK#S demonstrated superior performance, likely due to its smaller particle size and higher surface area. The study establishes that *M. koenigii* is an effective and sustainable source for the green synthesis of SnO_2 nanoparticles. Moreover, the selection of specific plant parts plays a critical role in modulating structural, thermal, and catalytic properties, making this method promising for environmental and catalytic applications.

Keywords: *Murraya koenigii*, Nanoparticle, Green Synthesis, Dye Degradation, Malachite Green.
RASĀYAN *J. Chem.*, Vol. 18, No.4, 2025

INTRODUCTION

Nanoparticles (NPs) have garnered substantial interest in recent years due to their remarkable properties that distinguish them from their bulk counterparts. These include unique optical, thermal, magnetic, and electrochemical characteristics, largely attributed to their nanoscale dimensions and high surface-area-to-volume ratio.[1-4] As a result, Nanoparticles are utilized across a broad range of applications, including environmental remediation, medicine, drug delivery, energy storage, catalysis, information technology, agriculture, heavy industries, and consumer products.[5-6] However, the conventional physical and chemical methods used for NP synthesis—such as the reduction of precursor salts in oil–water microemulsions, use of ionic liquids, pulsed laser ablation, thermal decomposition, microwave irradiation, and chemical reduction—often involve hazardous reagents and generate toxic by-products, thereby posing serious health and environmental concerns.[7-9] In light of these drawbacks, green synthesis approaches have emerged as viable and sustainable alternatives. These eco-friendly methods are aligned with the principles of green chemistry and involve the use of natural resources such as plant extracts, bacteria, fungi, and algae, eliminating the need for harmful chemicals while offering cost-effective and scalable synthesis routes. Among these green synthesis methods, plant-mediated synthesis has received particular attention due to its simplicity, biocompatibility, and environmental friendliness. As highlighted by Sankarganesh *et al.* plant extracts play a dual role in this approach by functioning as both reducing and capping agents. These extracts are rich in phytochemicals such as alkaloids, amino acids, ascorbic acid, oxalic acid, carboxylic acids, polyphenols, flavonoids, alcohols, terpenoids, glycosides, carbohydrates, thiamine, vitamin C, and polyols, which facilitate the reduction of metal ions and stabilization of the synthesized nanoparticles.[10-14]

http://doi.org/10.31788/RJC.2025.1849407

The biological activity and physicochemical behavior of inorganic nanoparticles are significantly influenced by factors such as particle size distribution, morphology, surface charge, surface chemistry, and particularly the nature of the capping agents. Capping agents stabilize the colloidal system, influence the particle's dispersion and interaction with living cells, and modify surface properties. For biomedical and environmental applications, it is crucial that these agents are biodegradable, biocompatible, biosoluble, non-toxic, and well-dispersed to ensure safe interaction with living systems and minimal ecological footprint.[15-20] In this context, plant-derived biomolecules are ideal, offering an environmentally safe and functionally effective alternative to synthetic surfactants. Among various metal oxide nanoparticles, tin oxide (SnO_2) NPs have attracted considerable attention due to their wide range of applications, including ultraviolet-visible (UV-Vis) sensitivity, electronics, catalysis, thermal conductivity, gas sensing, and antimicrobial activity. According to Matussin *et al.* SnO_2 NPs have been successfully synthesized using different plant extracts, supporting the potential of green methods for producing functional nanomaterials.[21] Owing to their excellent physicochemical properties, SnO_2 NPs are particularly promising for use in catalysis, water purification, sensors, lithium-ion batteries, and environmental remediation.[10,21] In the present study, a green synthesis approach has been adopted using different parts of the *Murraya koenigii* plant—commonly known as the curry tree and belonging to the Rutaceae family—which is widely distributed in tropical and subtropical regions. *Murraya koenigii* is well-known for its phytochemical richness, with its leaf, stem, and root extracts containing bioactive compounds such as cinnamaldehyde, various carbazole alkaloids, and antioxidants including tocopherol, carotene, and lutein. These phytochemicals serve as natural reducing and stabilizing agents, making the plant an excellent candidate for the green synthesis of SnO_2 nanoparticles. The objective of this study is to fill this research gap by synthesizing SnO_2 NPs using the leaf, stem, and root extracts of *Murraya koenigii* and evaluating the influence of each extract on the properties of the resulting nanoparticles. To comprehensively analyze the synthesized nanoparticles, various advanced characterization techniques have been employed. These include X-ray diffraction (XRD) for crystallographic analysis, field emission-scanning electron microscopy (FE-SEM) for morphological and particle size investigation, energy-dispersive X-ray spectroscopy (EDAX) for elemental composition, Fourier-transform infrared spectroscopy (FT-IR) for identifying functional groups, and thermal analysis (TGA and DTG) to assess thermal stability. These techniques provide a comprehensive understanding of the structural, morphological, compositional, and functional attributes of the SnO_2 nanoparticles synthesized using different parts of *Murraya koenigii*. This study highlights the potential of *Murraya koenigii* as an effective bioreducing and stabilizing agent, demonstrating its promise in the development of green nanotechnology solutions for sustainable applications.

EXPERIMENTAL

Aqueous solutions of tin chloride dihydrate ($SnCl_2 \cdot 2H_2O$) were prepared with a molar concentration of 1.27×10^{-5} M. For the green synthesis, 50 mL of freshly prepared *Murraya koenigii* (curry plant) extractobtained separately from the leaf, stem, and root was added dropwise into 200 mL of the $SnCl_2$ solution under constant stirring. The reaction mixture was maintained at 60 °C for 1 hour on a magnetic hotplate stirrer. A gradual color change from light green to brown indicated the formation of SnO_2 nanoparticles. The resulting colloidal solution was centrifuged at 15,000 rpm for 15 minutes, followed by repeated washing with distilled water to remove any unreacted precursors or plant residues. The purified nanoparticles were dried in a hot air oven. The synthesized SnO_2 nanoparticles were characterized using UV–Visible spectroscopy, X-ray diffraction (XRD), Fourier-transform infrared spectroscopy (FTIR), and scanning/transmission electron microscopy (FESEM) to evaluate their structural and morphological properties.

RESULTS AND DISCUSSION

UV Analysis

The UV–Visible absorption spectra of green-synthesized SnO_2 nanoparticles prepared from different parts of the *Murraya koenigii* (curry) plant—leaf (SnO_2-MK#L), stem (SnO_2-MK#S), and root (SnO_2-MK#R) are presented in Fig.-1. All samples exhibit strong absorption in the UV region below 400 nm, characteristic of SnO_2 nanoparticles, confirming successful formation. A noticeable blue shift in the absorption edge compared to bulk SnO_2 indicates the influence of quantum confinement effects, a hallmark of nanoscale

materials. The absorption onset varies slightly among the samples, suggesting that the phytochemical content in different plant parts influences nanoparticle morphology and size. Using Tauc's plot (not shown), the optical bandgap energies were estimated to be in the range of ~3.5–4.0 eV, which are slightly higher than that of bulk SnO_2 (~3.6 eV). This increase further supports the nanoscale nature of the synthesized particles and highlights the effectiveness of the green synthesis approach using *Murraya koenigii* extracts.

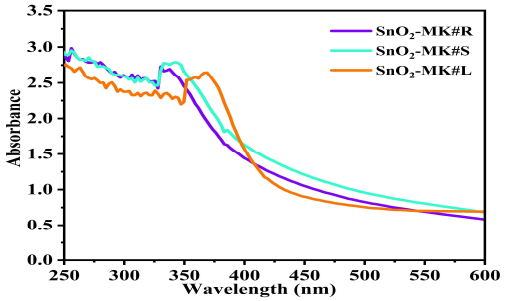

Fig.-1: UV–Visible Absorption Spectra of Green-Synthesized SnO_2 Nanoparticles Prepared Using Different Parts of the *Murraya koenigii* (curry) Plant: Root (SnO_2-MK#R), Stem (SnO_2-MK#S), and Leaf (SnO_2-MK#L)

X-Ray Diffraction

The crystalline structure and phase purity of the green-synthesized SnO_2 nanoparticles were investigated using X-ray diffraction (XRD), as shown in Fig.-2(A). The diffraction patterns of all three samples—SnO_2-MK#S (stem extract), SnO_2-MK#L (leaf extract), and SnO_2-MK#R (root extract)—exhibited well-defined peaks corresponding to the tetragonal rutile structure of tin oxide (SnO_2). These peaks closely match the standard JCPDS data (Card No. 00-041-1445), confirming the formation of a pure SnO_2 phase without any noticeable secondary phases or impurities. The characteristic diffraction peaks observed at 2θ values around 26.6°, 33.9°, 37.9°, 51.8°, and 54.7° respectively. The presence of sharp and intense peaks indicates a high degree of crystallinity in the synthesized materials. Simultaneously, the broadening of these peaks suggests the formation of nanoparticles with nanoscale dimensions. The crystallite size was estimated using the Debye–Scherrer equation, which yielded average sizes of approximately 12 nm for SnO_2-MK#S, 14 nm for SnO_2-MK#L, and 16 nm for SnO_2-MK#R. These differences in crystallite size can be attributed to the distinct phytochemical compositions and reducing potentials of the various parts of the *Murraya koenigii* plant. Notably, the root-derived nanoparticles (SnO_2-MK#R) exhibited slightly larger crystallite sizes, possibly due to the stronger aggregation tendency or variation in bioactive compounds. These results confirm that the green synthesis approach using curry plant extracts effectively facilitates the formation of crystalline SnO_2 nanoparticles in the nanometer range. Furthermore, the ability to modulate crystallite size through the selection of different plant parts highlights the versatility and tunability of this eco-friendly synthesis method.

Morphological and Elemental Analysis (FESEM and EDS)

The surface morphology of the green-synthesized SnO_2 nanoparticles was investigated using scanning electron microscopy (SEM), and the corresponding images for samples derived from leaf (SnO_2-MK#L), root (SnO_2-MK#R), and stem (SnO_2-MK#S) extracts of *Murraya koenigii* are presented in Fig.-2(B–D). The SEM image of SnO_2-MK#L [Fig.-2(C)] reveals a highly agglomerated, porous, and granular surface with interconnected nanoscale structures. In contrast, SnO_2-MK#R [Fig.-2(D)] shows larger, more faceted particles with a somewhat compact morphology, suggesting a different growth mechanism likely influenced by the bioactive compounds in the root extract. The SnO_2-MK#S sample [Fig.-2(B)] displays a relatively uniform distribution of spherical nanoparticles anchored on a larger background matrix, indicating partial particle aggregation and moderate crystallinity. The distinct morphologies observed across the three samples can be attributed to variations in the phytochemical composition of the plant extracts used during synthesis, which act as both reducing and capping agents. These structural differences may further influence surface area and catalytic activity in potential applications. The elemental composition of the synthesized SnO_2 nanoparticles was confirmed by energy-dispersive X-ray spectroscopy (EDS), as shown in Fig.-2(E). The spectrum exhibits prominent peaks corresponding to tin (Sn) and oxygen (O), confirming the formation of SnO_2. Minor peaks corresponding to carbon (C) are also observed, likely originating from the organic

components of the plant extract or from the carbon-coated sample holder. The absence of any other impurity peaks indicates the high purity of the green-synthesized SnO_2 nanoparticles.

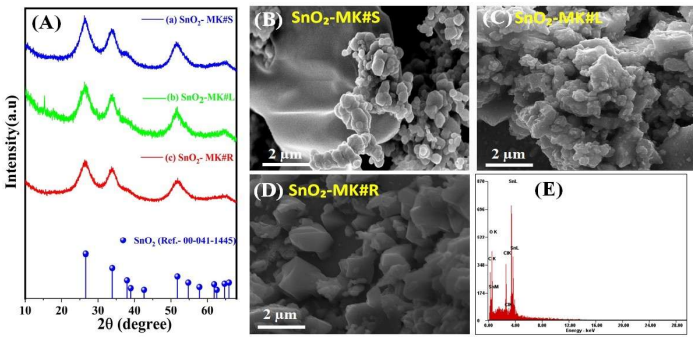

Fig.-2: XRD Patterns and SEM Micrographs of Green-Synthesized SnO_2 Nanoparticles using Murraya koenigii Extracts: A(a–c) Show XRD Patterns Confirming the Tetragonal Rutile Phase of SnO_2 (JCPDS 00-041-1445) with Crystallite Sizes Ranging from 12–16 nm; (B–D) SEM Images Reveal Distinct Morphologies Influenced by Root, Stem, and Leaf Extracts; (E) EDS Spectrum Confirms Elemental Composition with Dominant Peaks of Sn and O

FTIR

The FTIR spectra of both *Murraya koenigii* (MK) extracts (leaf, stem, and root) and the corresponding SnO_2 nanoparticles (SnO_2-MK#L, SnO_2-MK#S, SnO_2-MK#R) provide insight into the functional groups involved in the synthesis and stabilization of the nanoparticles, as shown in Fig.-3. In the spectra of plant extracts (MK#L, MK#S, MK#R), broad absorption bands observed around 3400 cm^{-1} can be attributed to O–H stretching vibrations of hydroxyl groups and inter/intramolecular hydrogen bonding, indicating the presence of polyphenols and flavonoids.[22] Peaks near 2920 cm^{-1} correspond to C–H stretching vibrations of aliphatic chains. Prominent bands at ~1630–1650 cm^{-1} are assigned to C=O or C=C stretching, typical of aromatic and carboxylic compounds, confirming the presence of various phytochemicals capable of acting as reducing and capping agents. The fingerprint region below 1500 cm^{-1} shows various peaks corresponding to C–O, C–N, and other functional group vibrations. In the case of SnO_2 nanoparticles, major absorption bands appear below 700 cm^{-1}, particularly around 620–480 cm^{-1}, which are attributed to Sn–O–Sn and Sn–O stretching vibrations. This confirms the successful formation of SnO_2 nanoparticles. The reduction in intensity or shifting of certain peaks in the nanoparticle spectra compared to their corresponding extracts indicates the interaction of plant biomolecules with the tin precursor during the synthesis process. These results suggest that phytochemicals present in *Murraya koenigii* play a crucial role in reducing Sn^{2+} to SnO_2 and simultaneously stabilize the nanoparticles, highlighting the green synthesis mechanism.

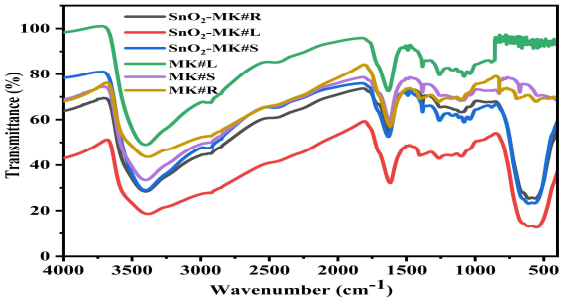

Fig.-3: FTIR Spectra of *Murraya koenigii* Extracts (MK#L, MK#S, MK#R) and their Corresponding SnO_2 Nanoparticles (SnO_2-MK#L, SnO_2-MK#S, SnO_2-MK#R)

Thermal Analysis

The thermal stability and decomposition behavior of green synthesized SnO_2 nanoparticles prepared using *Murraya koenigii* extracts—root (SnO_2-MK#R), stem (SnO_2-MK#S), and leaf (SnO_2-MK#L)—were investigated through Thermogravimetric Analysis (TGA) and Derivative Thermogravimetric Analysis (DTG), as shown in Fig.4-(a-c). All three samples exhibited multi-step weight loss patterns, reflecting the

presence and decomposition of phytoconstituents from the respective plant parts. SnO_2-MK#R exhibited three distinct weight loss stages: an initial 11.58% loss from 54–272 °C attributed to moisture and volatile compounds, followed by a 12.55% loss between 272–476 °C due to the decomposition of organic residues, and a final 13.08% loss up to 890 °C associated with residual carbonaceous matter.[20] The total residue remaining was 54.27%. SnO_2-MK#S displayed comparatively higher thermal stability, with four degradation steps. The initial 8.42% loss at 100–184 °C was followed by 7.11% and 4.51% weight losses at 313–451 °C due to the breakdown of phytochemicals, and a final minor loss of 2.84% at higher temperatures (~809 °C). The highest residual mass (77.09%) indicated enhanced thermal resistance, possibly due to the nature and amount of organic content from the stem extract. SnO_2-MK#L also underwent three degradation phases. The first stage (32–208 °C) accounted for 9.36% weight loss from adsorbed water and volatiles, the second (308–578 °C) showed an 8.92% loss attributed to phytochemical degradation, and a final 4.65% loss occurred up to 860 °C. The residue obtained was 69.23%. Overall, the differences in thermal degradation behavior and residue content can be ascribed to the varying compositions of bioactive compounds present in the root, stem, and leaf extracts. Among the three, SnO_2-MK#S exhibited superior thermal stability, making it potentially more suitable for high-temperature applications.

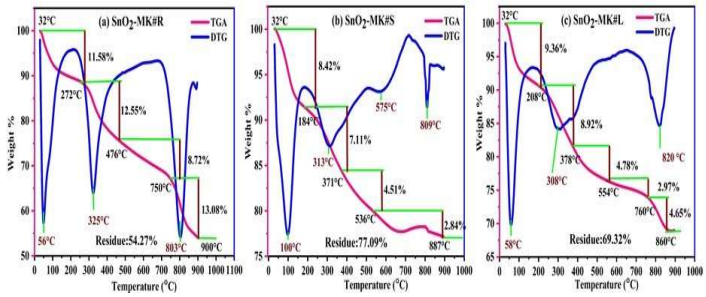

Fig.-4: TGA and DTG Curves of SnO_2 Nanoparticles Showing Multi-Step Thermal Degradation Behavior and Corresponding Residue Percentages

Catalytic Activity of Synthesized SnO_2 Nanoparticles in the Degradation of Malachite Green

The catalytic potential of green-synthesized SnO_2 nanoparticles was evaluated for the degradation of malachite green (MG) dye under alkaline conditions (pH 8) at room temperature. The reaction progress was monitored at λ_max = 600 nm. As shown in Fig.-5, a linear relationship was observed between the initial rate of reaction $(da/dt)_t$ and the concentration of catalyst, indicating a first-order dependence on catalyst loading. Among the three nanoparticle variants—SnO_2-MK#L (leaf), SnO_2-MK#R (root), and SnO_2-MK#S (stem)—the SnO_2-MK#S exhibited the highest catalytic activity. This can be attributed to the smaller particle size of the stem-derived nanoparticles, which likely provided a higher surface area and more active sites, thereby enhancing their catalytic efficiency in the degradation of malachite green.

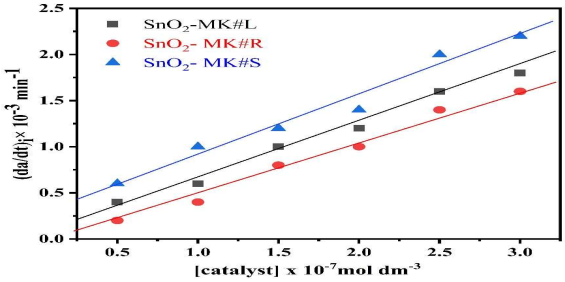

Fig.-5: Effect of SnO_2-MK#L, MK#R, and MK#S Catalyst Concentration on the Rate of Malachite Green Degradation. SnO_2-MK#S Shows the Highest Activity Due to Its Smaller Particle Size

CONCLUSION

In the present study, tin oxide (SnO_2) nanoparticles were successfully synthesized via a green, eco-friendly route using aqueous extracts from different parts (leaf, stem, and root) of *Murraya koenigii*. The synthesized nanoparticles were thoroughly characterized by UV–Vis spectroscopy, XRD, FTIR, SEM–EDS, and TGA/DTG. XRD confirmed the formation of highly crystalline SnO_2 with a tetragonal rutile structure and

particle sizes in the nanometer range. SEM images revealed morphological variations influenced by the source of plant extract, while EDS confirmed elemental purity. FTIR analysis indicated the involvement of phytochemicals in the reduction and stabilization of SnO_2 nanoparticles. Thermal analysis demonstrated that stem-derived SnO_2 (SnO_2-MK#S) exhibited the highest thermal stability, with a residual mass of 77.09%, indicating its potential suitability for high-temperature applications. Furthermore, catalytic studies revealed that SnO_2-MK#S also showed superior catalytic performance in the degradation of malachite green dye, which is attributed to its smaller particle size and higher surface activity. These findings validate the efficiency of *M. koenigii* as a green reducing and stabilizing agent and highlight the significance of plant part selection in tailoring nanoparticle properties for targeted environmental and catalytic applications.

ACKNOWLEDGMENTS

The XRD, FESEM, TGA, and FTIR facilities provided by IIT Roorkee, for which the authors are grateful. The UV-Vis spectrometers was provided by Invertis University Bareilly. The authors also express their gratitude to these organizations.

CONFLICT OF INTERESTS

The authors declare that there is no conflict of interest.

AUTHOR CONTRIBUTIONS

The present work is related to *SDG-12: Responsible Consumption and Production*. All the authors contributed significantly to this manuscript, participated in reviewing/editing and approved the final draft for publication. The research profile of the authors can be verified from their ORCID ids, given below:

Priya Gupta https://orcid.org/0009-0009-1878-4054
Hira Ilyas https://orcid.org/0009-0007-4795-6615
D. S. Raghav https://orcid.org/0009-0005-0540-6071
Sudha Tomar https://orcid.org/0000-0002-1219-133X

REFERENCES

1. K.N. Thakkar, S.S. Mhatre, R.Y. Parikh, *Nanomedicine: Nanotechnology, Biology, and Medicine,* **6(2)**, 257(2010), https://doi.org/10.1016/j.nano.2009.07.002
2. T. Nesakumar, J. Immanuel, Y. Rok, M. Gopalakrishnan, *Spectrochimica Acta Part A: Molecular and Biomolecular Spectroscopy,* **161(2)**, 122(2016), https://doi.org/10.1016/j.saa.2016.02.044
3. Mahalakshmi Lakshmanan, Dharani Ragul, Maria Leena Michael, Jeyan Arthur Moses, Chinnaswamy Anandharamakrishanan, *Letter in Applied Nanobio Science*, **11(2)**, 3411(2022), https://doi.org/10.33263/LIANBS112.34113420
4. G. GnanaJobitha, S. Rajeshkumar, G. Annadurai, C. Kannan, *Journal of Environmental Nanotechnology*, **2(1)**, 4(2013), https://doi.org/10.13074/jent.2013.02.121023
5. T. Jebakumar Immanuel Edison, M.G. Sethuraman, *Process Biochemistry*, **49(9)**, 1351(2012), https://doi.org/10.1016/j.procbio.2012.04.025
6. X. Zhang, K. Chan, *Chemistry of Materials*, **15**, 451(2003), https://doi.org/10.1021/cm0203868
7. V.A. Zuñiga-Ibarra, S. Shaji, B. Krishnan, J. Johny, S.S. Kanakkillam, D.A. Avellaneda, J.A.A. Martinez, T.K. Das Roy, N.A. Ramos-Delgado, *Applied Surface Science* **483**, 156(2019), https://doi.org/10.1016/j.apsusc.2019.03.302
8. Masoud Salavati-Niasari, Fatemeh Davar, Noshin Mir, *Polyhedron*, **27(17)**, 3514(2008), https://doi.org/10.1016/j.poly.2008.08.020
9. S.V. Otari, R.M. Patil, S.J. Ghosh, S.H. Pawar, *Materials Letters*, **116**, 367(2014), http://dx.doi.org/10.1016/j.matlet.2013.11.066
10. P.S.A. Ganesh, K. V Parthasarathy, B. Joseph, G.P.R. Anbarasan, *Journal of Inorganic and Organometallic Polymers and Materials*,**31,** 2971(2021), https://doi.org/10.1007/s10904-021-01894-6

11. M. Jha, S. Ansari, N.G. Shimpi, *Journal of Industrial and Engineering Chemistry* **69**, 269(2019), https://doi.org/10.1016/j.jiec.2018.09.030
12. S. Bhattacharjee, F. Habib, N. Darwish, A. Shanableh, *Powder Technology*, **380**, 219(2021), https://doi.org/10.1016/j.powtec.2020.11.055
13. S.O. Aisida, N. Madubuonu, M.H. Alnasir, I. Ahmad, S.B.M. Maaza, *Applied Nanoscience*, **10(1)**, 305(2020), https://doi.org/10.1007/s13204-019-01099-x
14. A. Khatua, A. Prasad, E. Priyadarshini, A. Kumar, P. Aparupa, *Journal Cluster Science*, **31(6)**, 1329 (2020), https://doi.org/10.1007/s10876-019-01742-1
15. P.R. Sougandhi, S. Ramanaiah, *Inorganic and Nano-Metal Chemistry*, **50(12)**, 1290(2020), https://doi.org/10.1080/24701556.2020.1745839
16. M. Kundu, G. Karunakaran, D. Kuznetsov, *Powder Technology,* **311(3)**, 132(2017), https://doi.org/10.1016/j.powtec.2017.01.085
17. V. Selvanathan, M. Aminuzzaman, L. Xian, Y. Foo, E. Seong, G. Cheah, M. Hsuan, L. Tey, S. Arullappan, N. Algethami, *Journal of Materials Research and Technology*, **20**, 2931(2022), https://doi.org/10.1016/j.jmrt.2022.08.028
18. H. Barabadi, H. Vahidi, M. Ali, M. Zahra, K. Kaveh, D. Kamali, *Journal of Cluster Science,* **31(6)**, 1173(2020), https://doi.org/10.1007/s10876-019-01733-2
19. K. Elumalai, S. Velmurugan, S. Ravi, V. Kathiravan, S. Ashokkumar, *Materials Science in Semiconductor Processing,* **34**, 365(2015), https://doi.org/10.1016/j.mssp.2015.01.048
20. A. Goel, S. Tomar, S. Tomar, *Journal of Nanostructures*, **10(4)**, 846(2020), https://doi.org/10.22052/JNS.2020.04.018
21. H.E. Garrafa-Galvez, O. Nava, C.A. Soto-Robles, A.R. Vilchis-Nestor, G. Elango, S. Manoj, S. Santhosh, S. Muthuraja, S. Mohana, A. Goel, S. Tomar, P. Suvaitha, S. Selvam, D. Ganesan, V. Rajangam, A. Raji, S. Matussin, M.H. Harunsani, A.L. Tan, M.M. Khan, K.C.S.S. Surendhiran, P.M. Kumar, E.R. Kumar, Y.A.S. Khadar, *Discover Applied Sciences*, **2(10)**, 354(2020), https://doi.org/10.1016/j.saa.2015.03.033
22. A. Goel, S. Tomar, *Inorganic and Nano Metal Chemistry*, **54(4)**, 342(2024). https://doi.org/10.1080/24701556.2022.2034016

[RJC-9407/2025]